Title

Neural correlates of unconscious and conscious visual processing

Maëlan Q. Menétrey[1,2,3], Michael H. Herzog[1], & David Pascucci[1,2,3]

[1]Laboratory of Psychophysics, Brain Mind Institute, École Polytechnique Fédérale de Lausanne (EPFL), Lausanne, Switzerland

[2]Psychophysics and Neural Dynamics Lab, Department of Radiology, Lausanne University Hospital (CHUV) and University of Lausanne (UNIL), Lausanne, Switzerland

[3]The Sense Innovation and Research Center, Lausanne, Switzerland

Keywords: consciousness, unconscious processing, two-stage model, neural correlates, EEG

Corresponding author: maelan.menetrey@gmail.com

Number of pages: 29

Number of figures: 5; of supplementary figure: 1

Number of words for abstract: 181; for introduction: 793; for discussion: 1122

Acknowledgments: This work was supported by the Swiss National Science Foundation (grant number 325130_204898; grant numbers PZ00P1_179988 and PZ00P1_179988/2; and grant number TMSGI1_218247).

Abstract

Postdictive effects, where later events influence the perception of earlier ones, suggest that conscious perception is not a continuous stream but occurs at discrete moments, preceded by extended periods of unconscious processing. This is evident in the Sequential Metacontrast Paradigm (SQM), where a stream of lines and vernier offsets is unconsciously integrated over several hundred milliseconds before conscious perception emerges: regardless of whether one or multiple verniers are shown, only a single offset is perceived from the first to the last line. Postdictive phenomena offer a unique opportunity to study the neural correlates of unconscious and conscious stages of perception because unconscious and conscious processing are well separated in time. Using EEG recordings during the SQM, we identified two distinct stages of neural activity. Early occipital EEG activity patterns (~200 ms after the initial vernier presentation) capture unconscious processing, while later centro-parietal EEG patterns (~400-600 ms after the onset of the stimulus stream) are associated with conscious perception, aligning closely with behavioral reports. We propose that the transition between these distinct neural topographies reflects the discrete moments when conscious perception emerges.

Introduction

Consciousness feels like a continuous stream; we see the world at each moment of time. However, several visual phenomena challenge this idea. For instance, in the color phi illusion, two dots of different colors are flashed at separate locations with a brief delay (Kolers & Von Grünau, 1976). Rather than perceiving two distinct flashes, we perceive a single moving dot that changes color midway. This color change can only be perceived after the second dot is presented, implying that later events influence how we perceive earlier ones. Postdictive effects, like the color phi illusion, suggest that conscious perception is not continuous but is preceded by a period of unconscious processing: consciousness is temporally discrete (Herzog et al., 2016, 2020). The discrete nature of consciousness provides a unique opportunity to study the neural correlates of both conscious and unconscious processing, as well as the transitions between the two, using high-temporal resolution imaging techniques like electroencephalography (EEG).

A prime tool for studying these processes is the Sequential Metacontrast (SQM) paradigm (Figures 1A and 1B). In this paradigm, a sequence of vertical lines is presented, creating the illusion of two diverging motion streams expanding from a central point (Otto et

al., 2009, 2010). When one of the lines contains a horizontal vernier offset, all the other lines are perceived as having the same offset, even though they are actually straight. Observers can easily report the vernier offset (left vs. right) but cannot identify which specific line carries the offset (Otto, 2006). When the stream contains two vernier stimuli with opposite offsets, the offsets *mandatorily* integrate, and only one integrated offset is perceived in the entire sequence —it is impossible to report the individual offsets separately (Drissi-Daoudi et al., 2019). The mandatory integration period spans approximately 330-450 ms, depending on the observer and the condition (Vogelsang et al., 2023). When two offsets are separated by longer intervals, observers can distinguish and report the individual offsets separately (Drissi-Daoudi et al., 2019; Vogelsang et al., 2023). Thus, the brain integrates events within a relatively long-lasting window of unconscious processing, followed by a discrete conscious percept. Then, the next window starts, encompassing a new unconscious period that leads to a discrete conscious percept. The existence of such long-lasting integration windows has been demonstrated not only in visual perception (Scharnowski et al., 2009; Mudrik et al., 2011; Marti & Dehaene, 2017; Sergent, 2018), but also in auditory perception (McWalter & McDermott, 2019) and across different sensory modalities (Fiebelkorn et al., 2010; Stiles et al., 2018; Rimsky-Robert et al., 2019).

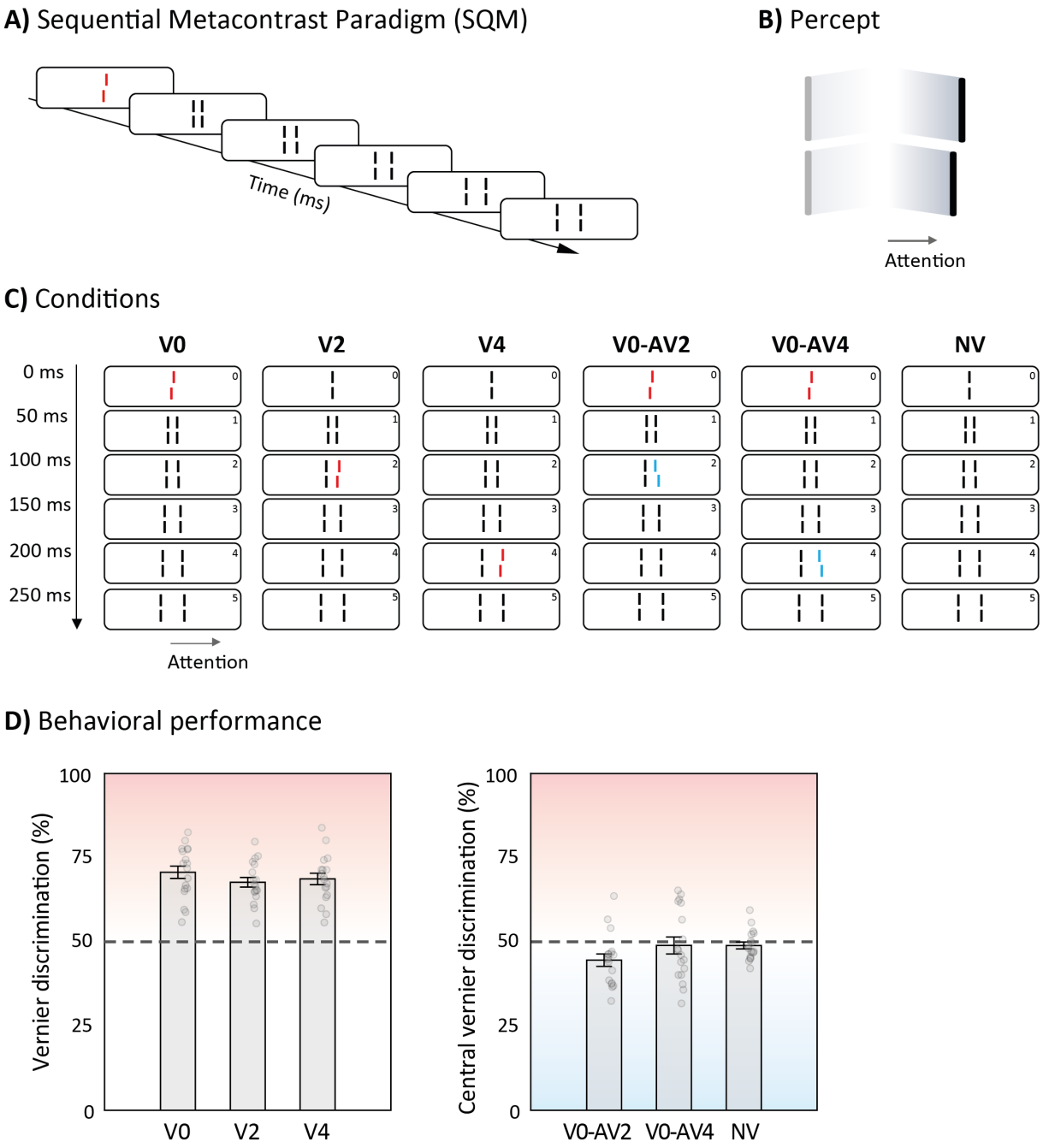

Figure 1. A) The Sequential Metacontrast paradigm (SQM). A central line, here with a vernier offset, is followed by pairs of flanking lines eliciting a percept of two diverging streams (B). Observers attend to one stream, in which all offsets are integrated. C) In V conditions, only one vernier is presented, either in the central line (V0), in the 2nd (V2), or in the 4th (V4) flanking line. In V-AV conditions, the central line is offset, and one of the flanking is offset in the opposite direction (anti-vernier; V0-AV2 or V0-AV4). In the control condition (NV), only straight lines are shown. The red and blue offset colors in the figure are for illustration purposes only; in the experiment, all lines were the same color. D) Participants attended to the right stream and were asked to report the perceived offset direction (right/left) of the 1st presented vernier offset by pressing hand-held push-buttons. In V conditions, participants could accurately report the offset direction. In V-AV conditions, participants could not perceive the individual vernier offsets, and hence performance is at 50%. This indicates that both vernier offsets contribute equally. When no vernier was presented or perceived, participants were guessing. In NV condition, performance is determined by comparing the response to a randomly chosen offset.

In this study, we used EEG decoding to investigate the neural mechanisms involved in both the unconscious processing of vernier offsets and the subsequent emergence of conscious perception, with the following rationale. In the SQM, independently of the exact temporal location or number of verniers in the stream, all offsets are accurately but unconsciously integrated. Only a single, integrated offset is consciously perceived. Consequently, neural activity patterns that can differentiate the position or number of offsets are attributed to unconscious mechanisms. In contrast, conscious perception emerges after unconscious processing and should reflect the integrated offset. To investigate this, we calibrated vernier offset sizes so that, in some trials where a vernier was presented alone in the stream, participants failed to consciously perceive the offset (incorrect trials), while in others, they correctly perceived it (correct trials). Thus, neural activity patterns that can distinguish between correct and incorrect trials within the same condition are likely associated with the conscious perception of the vernier.

Results

Unconscious feature integration within the SQM stream

Participants consistently integrated the vernier offsets with all the lines in the stream, regardless of how many offsets were present, i.e., individual elements in the SQM stream could not be perceived separately (Figure 1A; Drissi-Daoudi et al., 2019; Vogelsang et al., 2023). For example, in the conditions with only a single vernier (V conditions), the offset was perceived as extending across the entire sequence of lines (Otto, 2006; Otto et al., 2010; Figure 1B), and offset discrimination performance was significantly above 50%. This effect was consistent regardless of where the offset appeared in the stream. When the offset occurred in the first central line or in the second or fourth flanking lines, the mean accuracy remained high (70% ± 7%). Paired t-tests comparing each of these V conditions with a no-vernier (NV) control condition resulted all in significant differences (all $p < .001$, Cohen's $d' > 3.3$; Figure 1D, left panel).

In contrast, when two opposite vernier offsets (a vernier and an anti-vernier) were included in the stream (V-AV condition, Figure 1C), the offsets were mandatorily integrated. Mean accuracy in reporting the first offset was 47% ± 9%, comparable to the NV condition (paired t-tests between the V-AV and NV conditions: all $p > .05$; Figure 1D, right panel). Thus, conscious perception does not depend on the position and number of offsets in the stream, as there is no conscious access to individual elements.

Neural representations preserve the chronology of events in the SQM stream

Even though conscious perception in the SQM results from the integration of all elements, we hypothesized that underlying neural activity patterns might still carry information about individual elements and their temporal sequence. To test this hypothesis, we applied Linear Discriminant Analysis (LDA) to decode the presence of vernier offsets and their temporal positions in the stream from EEG activity patterns.

We ran separate LDA classifiers to discriminate between trials with no offset (NV condition) and trials with a single vernier offset presented at different temporal positions in the stream (V0: 0 ms, V2: 100 ms, V4: 200 ms, Figure 1C). The classifiers successfully discriminated the presence of a vernier offset in all V conditions (Area Under the Curve, AUC > 0.5, cluster-based permutation test, $p < .05$; Figures 2A and 2B). Crucially, the decoding results revealed systematic delays that corresponded to the actual position of the vernier offset in the stream—decoding was successful at 240 ms for V0 vs. NV, at 330 ms for V2 vs. NV, and at 370 ms for V4 vs. NV (Figure 2B). Hence, the presence of an offset was decoded approximately 200 ms (170-240 ms) after the vernier's physical onset, despite participants perceiving the offset as present along the entire stream from the beginning (e.g., starting at 0 ms). This result was further supported by a temporal generalization analysis, in which we trained the classifier on data from each time point and tested it across all other time points (see Methods). This analysis revealed similar patterns across conditions, with decoders generalizing only over short time windows, as indicated by higher decoder performance when both training and testing occurred at the same time points (i.e., the diagonal elements of the temporal generalization matrices), and decoding latencies shifted depending on the vernier offset location (Figure 2A).

We then applied cross-condition decoding, training a classifier on discriminating V2 vs. NV or V4 vs. NV and testing it on V0 vs. NV. This revealed shared neural representations of the single vernier across conditions, but shifted along the diagonal in the cross-condition temporal generalization matrix (Figure 2C). Specifically, a decoder trained to detect the vernier in the V2 or V4 condition successfully decoded it in V0 (AUC > 0.5, cluster-based permutation test, $p < .05$), but with earlier onsets of approximately 100 and 200 ms, respectively. This delay decreased over time, with neural representations of the vernier offset in V0 gradually aligning with the temporal dynamics of V2 or V4 at longer latencies (e.g., after ~600 ms).

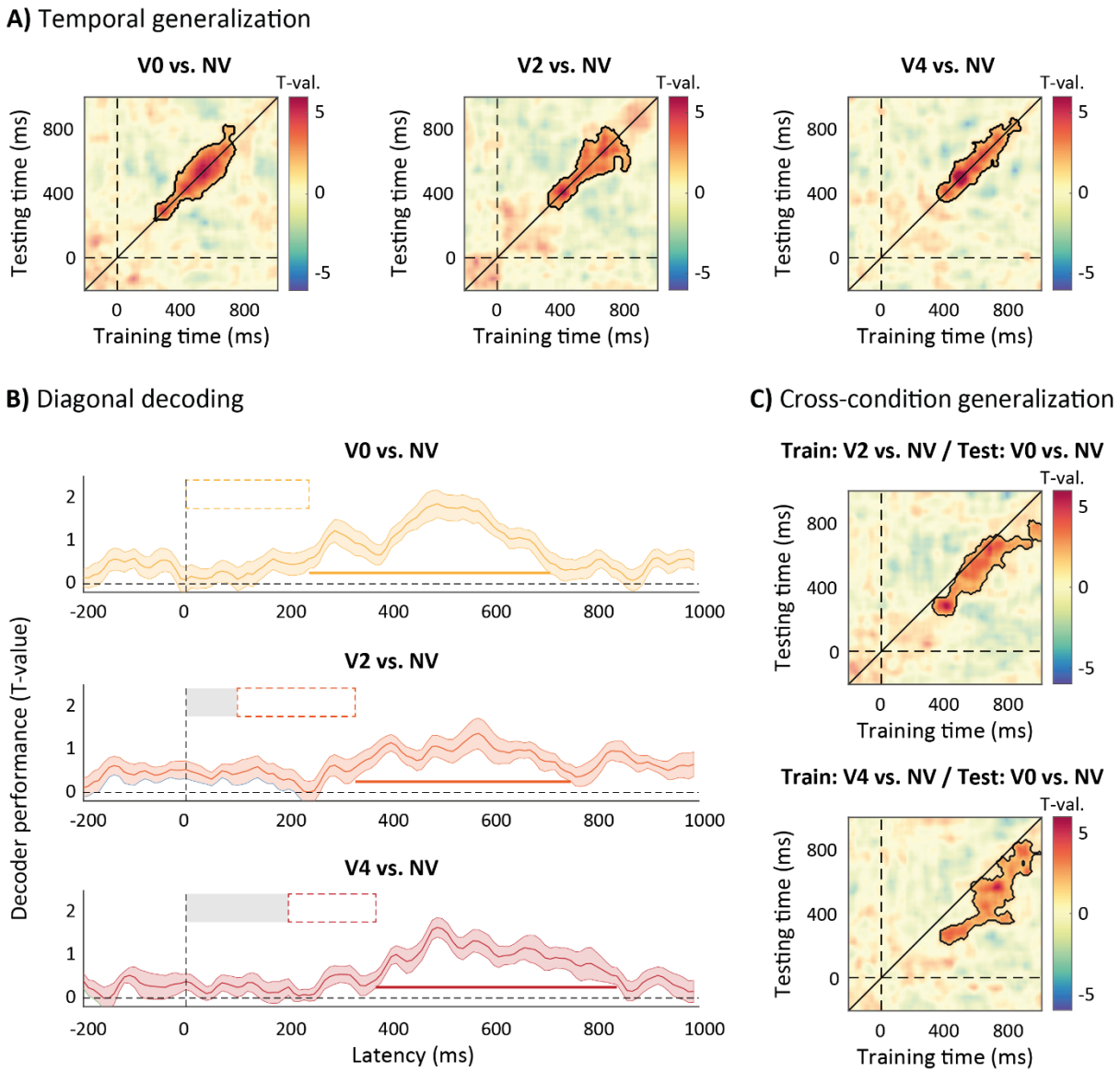

Figure 2. Linear discriminant analysis (LDA) with temporal and cross-condition generalization in V conditions. A) Temporal generalization matrices, obtained by training a classifier on data at every time point and testing it at all other time points, showing that classifiers can successfully discriminate between the conditions (V0, V2, and V4 vs. NV). Significant clusters are highlighted (AUC above 0.5, cluster-based permutation test, $p < .05$). B) Diagonal elements of the temporal generalization matrices, representing decoding results when training and testing at the same time point (group average AUC and 95% CI). Significant time windows are highlighted by the horizontal lines at the bottom. Temporal delays in the decoding results, relative to the actual onset of the vernier in the stream, are indicated by the dashed rectangles. C) Cross-condition generalization matrices demonstrate that classifiers trained with V2 or V4 vs. NV successfully discriminate V0 vs NV but with earlier onsets corresponding to the effective stimulus delay between V0 and V2 (i.e., 100 ms later) and V4 (i.e., 200 ms later). Significant clusters are highlighted (AUC above 0.5, cluster-based permutation test, $p < .05$).

Decoding the single vernier versus no vernier conditions was significant in windows ranging from 240 to 710 ms in V0 vs. NV, 330 to 750 ms in V2 vs. NV, and 370 to 840 ms in V4 vs. NV). In these time windows, we found two distinct EEG activation patterns—i.e., topographies of EEG activity associated with the decoder results (see Methods and Figure 3A).

The first topography displayed stronger activation over occipital electrodes, with increasing duration as the vernier offset occurred later in the stream (Figure 3B). The second topography, which showed increased activation over parietal electrode sites, had a shorter duration when the vernier offset occurred later (Figure 3B). The time course of these topographies, estimated by back-projecting activation patterns onto the original EEG time series, revealed a clear transition between the two patterns, with evident temporal shifts across conditions (i.e., the transition occurred around 360 ms in V0 vs. NV, 460 ms in V2 vs. NV, and 570 ms in V4 vs. NV; Figure 3C).

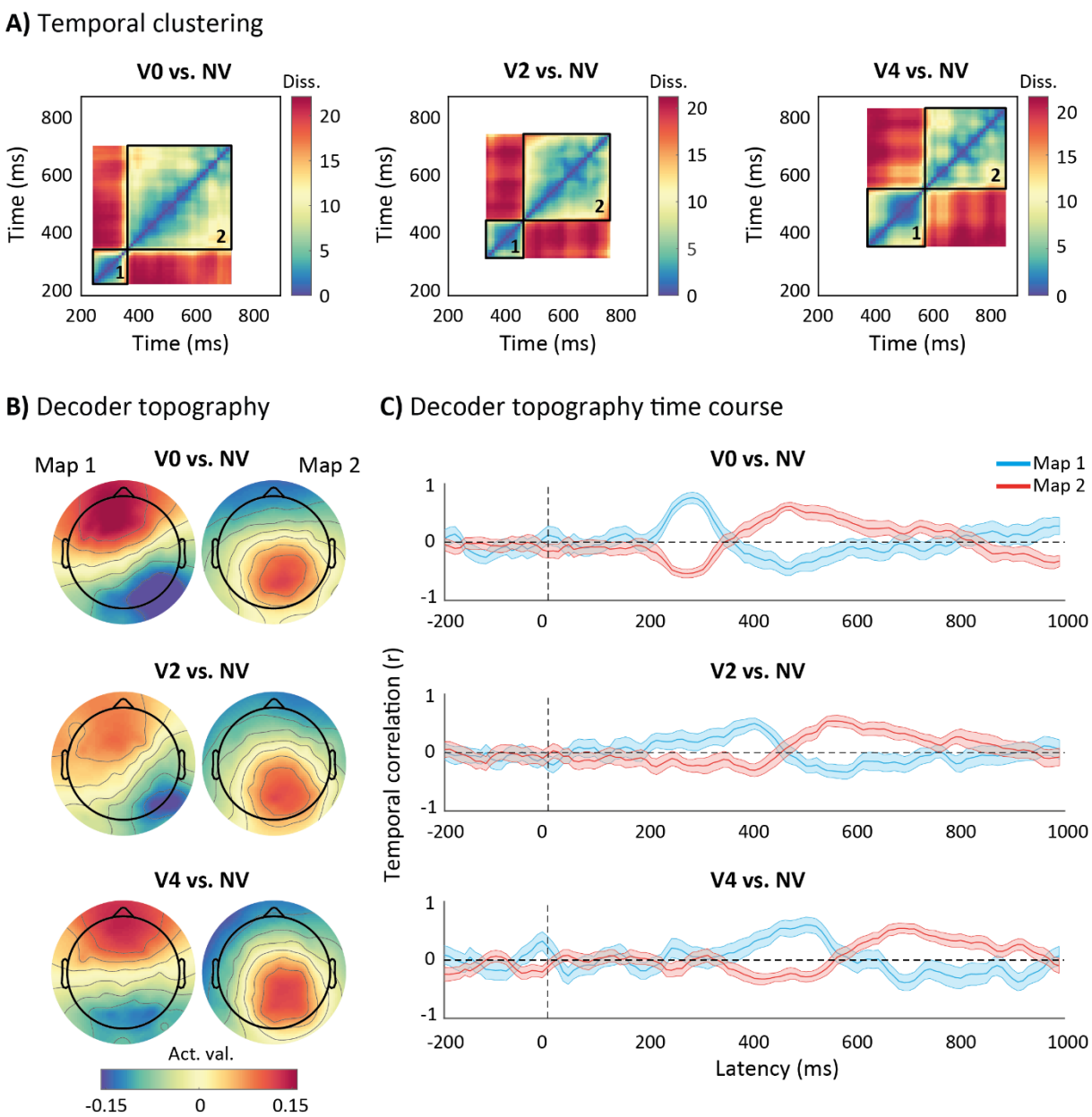

Figure 3. EEG activation patterns contributing to decoding in V conditions. A) Analysis of dissimilarity matrices between the EEG activation patterns extracted from significant time points (diagonal elements of the temporal generalization matrices for V0, V2, or V4 vs. NV; see Figure 2B) reveals two main activation patterns (outlined by black squares) for each decoding analysis. B) Topographies, averaged across participants, are derived from the two main activations patterns identified with the analysis of dissimilarity matrices. Each decoding analysis shows similar topographical maps but with variations in their transition dynamics. C) Temporal correlations between the two identified topographies and the back-projected time course of EEG activation patterns for each decoding analysis. Blue and red lines represent the 1st and 2nd maps, respectively. Shaded areas indicate SEM.

Neural correlates of unconscious processing

Up to this point, we have focused on conditions featuring a single vernier, where the vernier is consciously perceived throughout the entire stream. Even though the location of the vernier was not consciously perceived, it could still be decoded via two distinct EEG topographies. Next, we explored conditions involving two opposite vernier offsets, separated by varying intervals (V0-AV2: 50 ms, V0-AV4: 150 ms; Figure 1C), using LDA to distinguish these conditions from a condition featuring only straight lines (NV).

In the V-AV conditions, behavioral performance was around 50%, indicating mandatory integration of the two opposite offsets (Figure 1D). If the two topographies found when decoding the V conditions from the NV condition reflected only the neural correlates of conscious perception, then we would expect no significant decoding for V-AV trials compared to NV trials. However, if one or both topographies are associated with unconscious processing, i.e., before the offsets integrate, we would expect significant decoding.

Consistent with the latter hypothesis, the decoder successfully discriminated V0-AV2 and V0-AV4 trials from NV trials (AUC > 0.5, cluster-based permutation test, $p < .05$; Figure 4A). The significant decoding window (170-1000 ms) exhibited the same sequence of EEG activation patterns (Figure 4B) as observed in the V0 vs. NV decoding analysis. The significant decoding onset, topographies, and transition dynamics around 370 ms (Figures 4A, 4C, and 4D) also closely mirrored those found in V0 vs. NV conditions (Figures 3B and 3C for comparison). Thus, EEG activation patterns distinguished the presence of two offsets from no offsets, even though the individual offsets were not consciously perceived.

Importantly, we also found that the two V-AV conditions, where the second offset occurred at different times (V0-AV2 vs. V0-AV4), could be decoded from V0 trials, where only a single vernier was shown and consciously perceived (AUC > 0.5, cluster-based permutation test, $p < .05$; Figure 4A). This indicates that neural representations of the second vernier offset were detectable from EEG patterns, even though this second offset was not consciously perceived. The decoding windows (from 300 ms for V0-AV2 vs. V0, and from 340

ms for V0-AV4 vs. V0) were compatible with the latencies observed in single vernier decoding, supporting the idea that neural representations of the second vernier were present.

Moreover, the two V-AV conditions, despite yielding identical conscious percepts, were reliably discriminated from each other (AUC > 0.5, cluster-based permutation test, $p < .05$; Figure 4A). That is, EEG activation patterns contained information about the temporal order of the second vernier, which was completely inaccessible to conscious report but decodable starting from 420 ms. Together, these results demonstrate the involvement of one EEG topography (Figure 4C), highly similar to the first occipital topography identified when decoding conditions with one or two offsets from trials without any offset (Figures 3B and 4C).

Based on these findings, we interpret the first topography as the neural correlate of unconscious processing of the vernier stimuli, occurring before the emergence of a conscious percept. Conversely, the presence of the second topography with a centro-parietal pattern when discriminating V-AV from NV trials (Figure 4C) suggests a second stage in which the integrated percept becomes available to consciousness. As previously suggested (Menétrey et al., 2023), one of the two vernier offsets might dominate the integrated percept in the V-AV condition. Thus, despite chance-level performance, percepts in the V-AV conditions differ from those in the NV condition (i.e., a straight line moving from the center to the periphery). The latencies and sequence of topographies when decoding two opposite verniers from none, which are similar to those observed in the single vernier condition (Figure 3B), support this non-uniform integration in V-AV, likely leading to the conscious perception of a smaller integrated vernier in the stream (see also Supplementary Figure 1 for additional cross-condition generalization evidence between V and V-AV conditions).

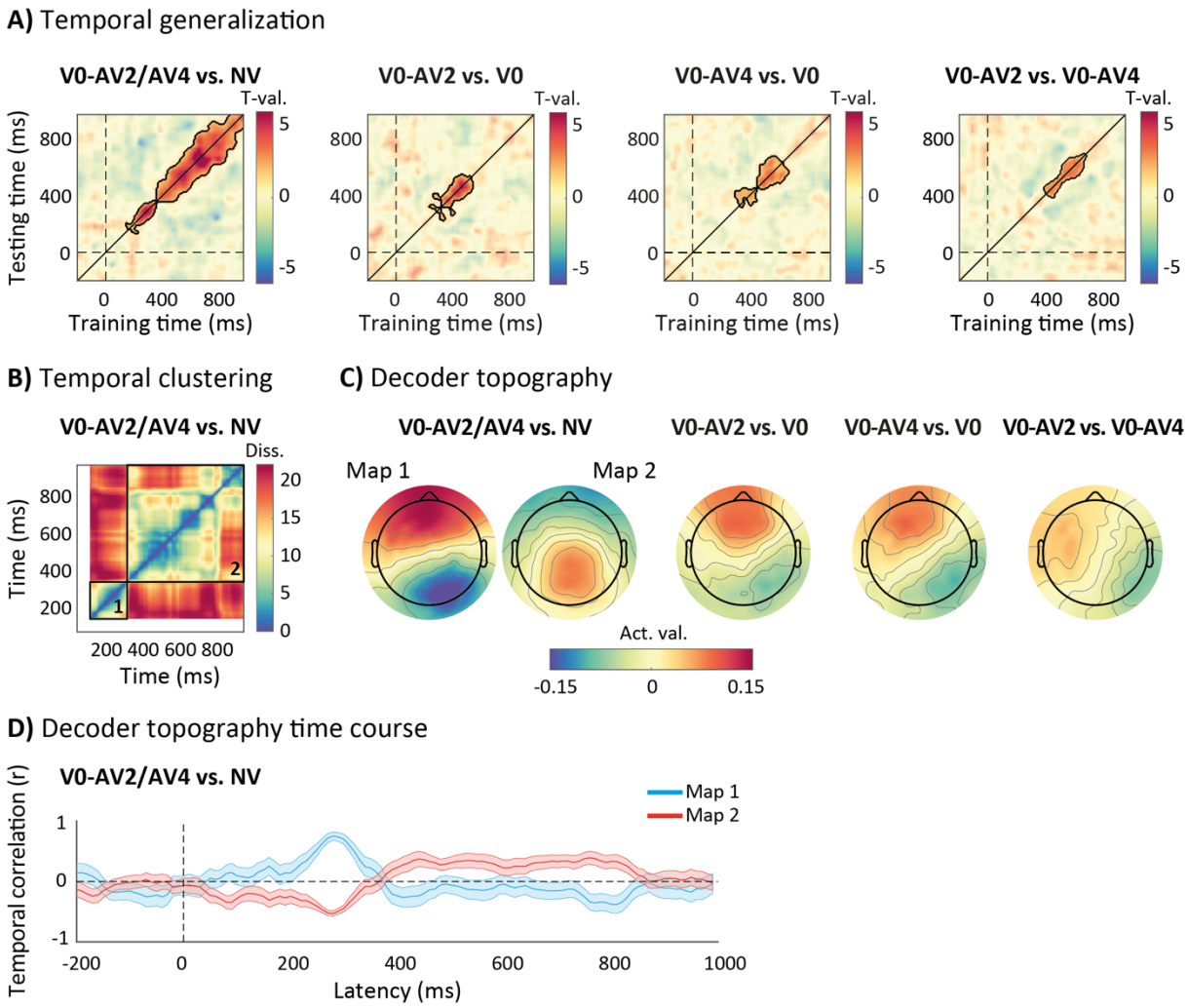

Figure 4. Linear discriminant analysis (LDA) with temporal and cross-condition generalization in V-AV conditions. A) Temporal generalization matrices showing that classifiers successfully discriminate the conditions (V0-AV2/V0-AV4 vs. NV, V0-AV2 vs. V0, V0-AV4 vs. V0, and V0-AV2 vs. V0-AV4). Significant clusters are highlighted (AUC above 0.5, cluster-based permutation test, $p < .05$). B) Analysis of dissimilarity matrices between the EEG activation patterns extracted from significant time points (diagonal elements of the temporal generalization matrices; see Figure 1A) reveals two different activation patterns (outlined by black squares) only for V0-AV2/V0-AV4 vs. NV. C) Topographies, averaged across participants, are derived from the two main activation patterns found in V0-AV2/V0-AV4 vs. NV. The topographies for V0-AV2 vs. V0, V0-AV4 vs. V0, and V0-AV2 vs. V0-AV4 are derived from the averaged activation pattern over the entire significant window. D) Temporal correlation between the two identified topographies and the back-projected time course of EEG activation patterns for V0-AV2/V0-AV4 vs. NV. Blue and red lines represent the 1st and 2nd maps, respectively. Shaded areas indicate SEM.

Neural correlates of conscious perception

To directly assess the involvement of the second topography in conscious perception, we applied LDA to decode correct versus incorrect reports of the offset direction in the condition featuring only a single vernier (V conditions). As shown in Figure 5, the classifiers successfully decoded behavioral performance in all single-vernier conditions (Figure 5A; AUC > 0.5, cluster-based permutation test, $p < .05$). However, significant decoding emerged at later

latencies —480 ms for V0, 460 ms for V2, and 570 ms for V4—compared to the earlier latencies observed when decoding V or V-AV against the no-vernier (NV) condition.

The decoding of the correctly reported direction was characterized by the contribution of a single EEG activation pattern, which perfectly aligned with the second topography identified in previous analyses (Figures 3B and 4C). This finding suggests that the later centro-parietal topography represents the neural correlate of the emergence of a consciously integrated percept, one that becomes available for report. The delayed decoding of correct versus incorrect responses, compared to the earlier decoding of vernier presence, indicates that this second topography is specifically linked to conscious awareness of the vernier offset, rather than its initial unconscious processing.

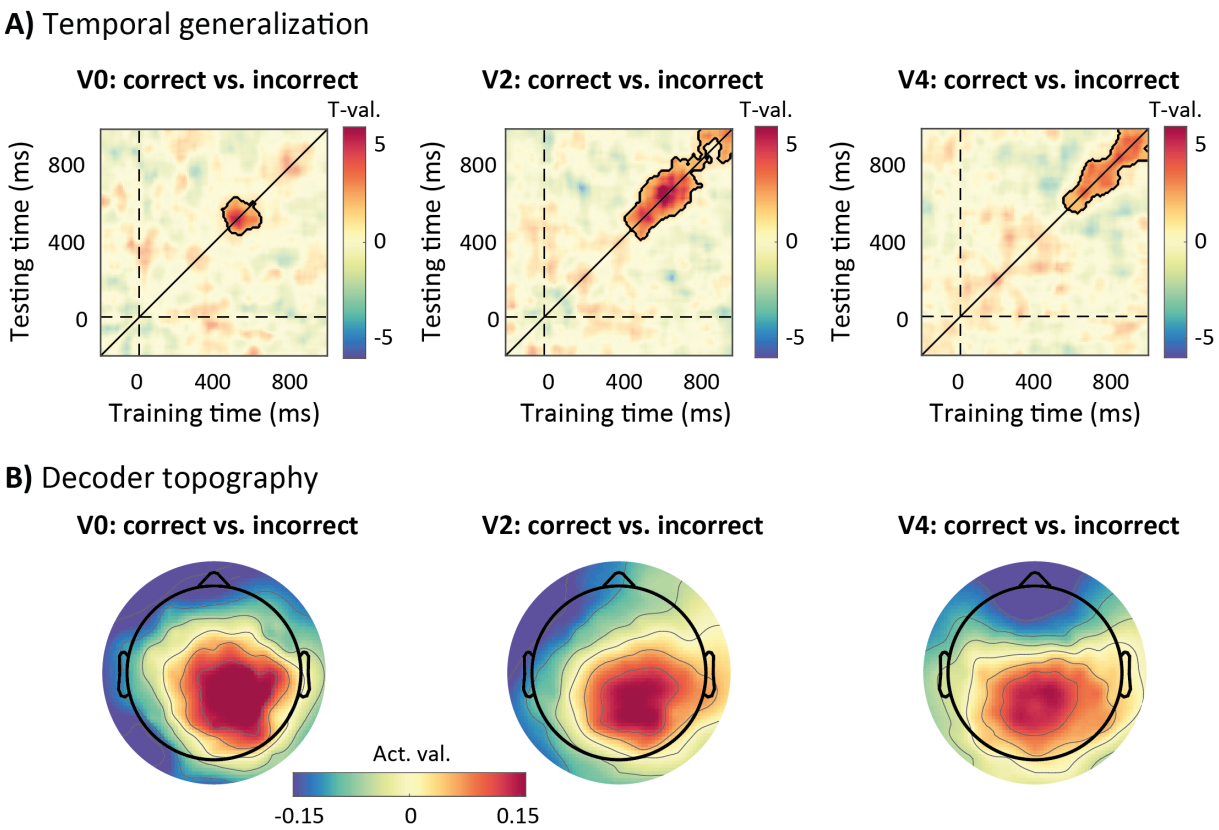

Figure 5. Linear discriminant analysis (LDA) with temporal generalization in V conditions (correct vs. incorrect reports). A) Temporal generalization matrices showing that classifiers ≈correct from incorrected offset reports in all V conditions (V0, V2 or V4). Significant clusters are highlighted (AUC above 0.5, cluster-based permutation test, $p < .05$). B) The topographies, averaged across participants, are derived from the averaged activation pattern over the entire significant window of each decoding analysis.

Discussion

Conscious perception is preceded by a period of unconscious processing (Herzog et al., 2016, 2020). This is evident in the SQM, where a sequence of lines and offsets is mandatorily and unconsciously integrated for up to 450 milliseconds before a conscious percept emerges (Drissi-Daoudi et al., 2019; Vogelsang et al., 2023). Here, we used time-resolved decoding analysis to investigate the EEG correlates of both unconscious and conscious processing within the SQM paradigm.

Conscious perception does not depend on the specific temporal location of the offsets in the stream, still, our findings show that unconscious neural representations retain the exact chronological order of vernier offset presentations, delayed by approximately 200 ms (Figure 2). This suggests that the brain retains detailed timing information about the offsets, even though this information remains inaccessible to conscious awareness, and contrasts with the unified conscious experience of a single moving offset. This conclusion is further supported by the fact that the temporal onset of individual verniers remained decodable in conditions with two opposite verniers, where the offsets mandatorily integrate and cannot be consciously perceived as separate (Figure 4). Thus, even when individual vernier offsets cannot be consciously perceived, their presence can still be inferred from EEG.

These decoding results were driven by early post-stimulus EEG activity, predominantly involving occipital signals (Figure 3). The corresponding EEG topography is consistent with findings from previous studies on the unconscious accumulation and integration of visual information (Fahrenfort et al., 2017; Menétrey et al., 2023) and aligns with the N170/VAN ERP component, which is associated with preconscious processes that engage attention for conscious perception (Koivisto & Revonsuo, 2010; Harris et al., 2013; Cohen et al., 2023). Interestingly, this topography was also observed when discriminating between conditions that resulted in a similar integrated conscious percept (i.e., a vernier offset moving along the entire stream) but involving different sequences of unconsciously processed events (i.e., one or two verniers; see Figure 4). Since these conditions differ in the location or even the number of physical offsets, this suggests that the early occipital topography reflects differences in the sequence of unconsciously processed events, supporting its role as a neural correlate of unconscious processing.

Following this early occipital activity, we found a second, more centro-parietal topography. This topography contributed to the decoding of conditions where one or more

vernier offset were compared against the condition with no offset, but was not observed when discriminating between one and two offsets. This suggests that this later topography is involved in the conscious perception of the vernier offset, whether it results from a single offset or the integration of two, compared to straight lines. In line with this, the same centro-parietal topography emerged after 460 ms and lasted several hundred milliseconds when decoding correct versus incorrect behavioral reports of the offset in conditions with a single vernier (see Figure 5). This late topography resembles the P300 ERP component, often linked to conscious access (Sergent et al., 2005; Polich, 2007; Rutiku et al., 2015; Silverstein et al., 2015), and is thought to signal the availability of information for conscious report (Baars, 2002). Since this centro-parietal topography only appeared when decoding the conscious perception of a single offset and correct reports, we interpret it as the neural correlate of conscious perception. Supporting this interpretation, similar topographies obtained through EEG decoding have also been associated with consciousness in attentional blink and masking paradigms (Weaver et al., 2019; Noorman et al., 2024). Alternatively, the second topography may not directly reflect the emergence of conscious perception, but rather cognitive processes associated with it, such as decision-making. However, its later occurrence and its relationship with correct reports suggest that, by the time this topography appears, the final percept of the entire sequence—resulting from the integration of unconsciously processed events—is available.

Our findings support a two-stage model of perception, in which a prolonged period of unconscious processing precedes a discrete conscious percept (Herzog et al., 2016, 2020). During the first stage, information is processed with high precision, preserving the temporal order and spatial details of events. In this phase, representations of each vernier offset are stored in a high-capacity buffer, where they interact unconsciously (Pang & Elntib, 2021, 2023). At the end of this unconscious processing window, the buffered information is collapsed into a conscious percept, reflecting the integrated structure of the entire event.

We show that these two stages involve distinct EEG topographies and underlying brain dynamics, with transitions closely aligning with the duration of unconscious processing windows previously reported from behavioral data (e.g., between 330 and 450 ms; Drissi-Daoudi et al., 2019; Vogelsang et al., 2023). Importantly, the duration of each stage and their transition dynamics are not fixed but depend on the timing of the first offset in the SQM stream. This was most evident when decoding a single vernier against no vernier (Figure 3). The first topography lasted slightly longer when the offset was presented later in the stream, while the second topography exhibited a temporal compression, shortening as the offset occurred later

(see Figure 3A). It is possible that the occurrence of a vernier offset contributes to the beginning of an unconscious processing window, while the end of the SQM stream may accelerate the collapsing of the sequence into a unified conscious percept. Indeed, offsets presented closer to the end of the entire stream (conditions V2, V4) might have accelerated the transition from unconscious to conscious processing. Although the nature of this stimulus-dependent temporal dynamic remains to be fully understood, these results suggest that the temporal structure of neural processing stages is flexible and influenced by subtle details of the stimulus sequence, in contrast to standard ERP analyses that often treat the latencies of processing stages as fixed.

Our results address the important question of when consciousness emerges. Most theories, with the exception of the global neuronal workspace theory (Dehaene et al., 2006; Dehaene & Changeux, 2011), do not clearly disentangle unconscious from conscious processing stages (for reviews, see Aru et al., 2012; Storm et al., 2017). In this respect, the two-stage nature of conscious perception —unconscious processing followed by a discrete percept— and the underlying neural mechanisms may provide strong constraints for these theories, leading to testable predictions. In particular, our results are of quantitative nature and thus allow precise testing of theories.

In sum, consciousness is not a continuous flow but is determined by transitions from extended periods of unconscious processing to moments of conscious perception. We demonstrate that during unconscious processing, the brain retains detailed temporal information about external stimuli, which is then integrated into a unified conscious percept where such temporal detail is no longer accessible. This transition between different functional brain states holds critical implications for future research aimed at characterizing the neural correlates of consciousness.

Methods

Participants

A total of 18 naive, healthy participants (9 females; age range: 18-23 years old) were recruited for the experiment. Participants had normal or corrected to normal vision, as assessed through the Freiburg acuity test (threshold for inclusion: >1; Bach, 1996). All participants signed informed consent before the experiment and received monetary compensation upon its completion. The experiment was conducted in accordance with the local ethics commission and complied with the Declaration of Helsinki (except for pre-registration).

Apparatus

The stimuli were presented on an ASUS VG248QE LCD monitor with a resolution of 1920 x 1080 pixels, a screen size of 24.5 inches, and a refresh rate of 144 Hz. MATLAB R2022b (MathWorks Inc., Natick, MA, USA) along with Psychtoolbox (Brainard, 1997) was used to generate the stimuli. During the experiment, participants were seated at a distance of 1.5 meters from the screen in a dimly lit room. The stimuli appeared as white with a luminance of 100 cd/m², displayed against a uniform black background with a luminance of 1 cd/m².

Stimuli and experimental procedure

We used the sequential metacontrast paradigm (SQM), introduced in Otto et al. (2006), which creates the perception of two motion streams diverging from the center (Figures 1A and 1B). The sequence always began with the presentation of a central vertical line, comprising an upper and a lower segment (the length of each segment is 26.6 arcmin, with a width of 1.2 arcmin) separated by a small vertical gap (2.5 arcmin). Next, pairs of flanking lines appeared progressively further away from the center (horizontal separation between each line is 5 arcmin). The central line and all subsequent pairs of lines were presented for 27.8 ms each, with an interstimulus interval (ISI) of 20.8 ms separating each presentation. The entire stimulus sequence consisted of one central and 5 flanking lines, lasting a total duration of 270.8 ms (Figure 1A).

Participants were instructed to always covertly attend to the right stream. In a randomized order, 6 different conditions were presented (Figure 1C): In the *no vernier* control condition (NV), all lines were straight. In three experimental conditions, one line of the attended stream was offset, with the lower segment shifted either towards the right or the left relative to

the upper segment (referred to as a *vernier offset* or V). In these conditions, the vernier offset was presented either in the 1st central line (V0 condition), in the 2nd flanker line (V2 condition; 100 ms after stimulus onset) or in the 4th flanker line (V4 condition; 200 ms after stimulus onset). In the two last conditions, the central line always had a vernier offset, while another line in the right stream was offset in the opposite direction (referred to as an *anti-vernier* or AV). In these conditions, the opposite vernier was presented either in the 2nd flanker line (V0-AV2 condition) or in the 4th flanker line (V0-AV4 condition).

In all conditions, participants were asked to indicate whether they perceived a left or right offset along the stream (Figure 1B), even when no vernier was presented (usually observers perceive the offset at the last line, even though the line was always straight). Observers were informed that one or two verniers could be presented in the stream and were instructed to report the 1st one in case they perceived both.

Participants completed a total of 12 blocks, with each block consisting of 96 trials (192 trials per condition). Before each trial, a central fixation point was presented for 250 ms, followed by an inter-stimulus interval of 750 ms. After the SQM presentation, participants had 3 seconds to give their response by clicking one of two hand-held buttons. If no response was made within this time, the trial was discarded and repeated at the end of the block. In order to eliminate potential early responses that occurred before the complete presentation of the stimulus sequence, we also excluded trials with reaction times below 300 ms after SQM onset. The inter-trial interval was set at 1 second.

Offset calibration

Before the experiment proper, the offset sizes (i.e., the horizontal displacement between their upper and lower segments) were determined to achieve comparable performance levels across participants. Streams of straight lines with one single vernier were presented, and a parameter estimation by sequential testing (PEST) procedure (Taylor & Creelman, 1967) was used to adaptively determine offset sizes leading to around 70% to 80% performance. This was performed with a vernier offset separately at the three different positions tested in the main experiment: the central line (V0), the 2nd flanker line (V2), or the 4th flanker line (V4).

Behavioral analysis

Performance was determined as the proportion of responses that matched the direction of the 1st presented vernier offset (Figure 1D). We compared performance between the NV condition

and each V or V-AV conditions by means of paired t-tests. The NV condition served as a baseline condition; in this condition performance was determined by comparing the response (left or right reported offset) to a randomly chosen notional offset (mean accuracy was 49% ± 4%). All statistical comparisons were Bonferroni-Holm corrected for multiple comparisons (bonf_holm()). When the vernier is presented without an anti-vernier, vernier discrimination should be approximately 75%, in line with the calibration performance. Conversely, when an anti-vernier follows the central vernier, the central vernier discrimination should be around 50%, given the integration of the two verniers. Additionally, we anticipated no performance differences related to the specific locations of the verniers and anti-verniers, as they fell within the same integration window (Drissi-Daoudi et al., 2019). Behavioral performance aligned with this expectation (see Results section).

Across the six tested conditions, average reaction times ranged from 885 ms to 920 ms, with no statistically significant difference between conditions (one-way ANOVA, $F(5, 102) = 0.08$, $p = .99$).

EEG recordings and preprocessing

The EEG data were recorded using a Biosemi Active Two system (Biosemi, Amsterdam, the Netherlands) with a total of 128 Ag–AgCl active electrodes, providing comprehensive scalp coverage. The positioning of the cap was adjusted individually to ensure the Cz electrode was equidistant from the inion and nasion, as well as equidistant from each ear. In addition, the electrooculogram (EOG) was recorded with 4 electrodes positioned 1 cm above and below the right eye and 1 cm lateral to the outer canthi. The recording was referenced to the CMS-DRL ground, maintaining the montage potential close to amplifier zero through a feedback loop. The sampling rate during recording was set at 2048 Hz.

For EEG preprocessing, EEGLAB was utilized (version v2021.1; Delorme et al., 2011; Delorme & Makeig, 2004). The EEG data were first downsampled to 250 Hz. To remove linear trends, detrending was applied (de Cheveigné & Arzounian, 2018), followed by a lowpass filter with a cutoff frequency of 40 Hz. The EEG data were then epoched from -1 s to 1.5 s relative to the onset of the SQM. To ensure data quality, a visual inspection was conducted to identify and exclude epochs (pre-selected with *pop_jointprob* function) or channels with significant noise or artifacts. Then, an ICA decomposition (*pop_runica* function with Picard algorithm; Ablin et al., 2017a, 2017b) was performed, with a temporary interpolation of the removed channels to maintain a consistent 128-channel configuration across all participants. The ICA

461 decomposition also included "fake" vertical and horizontal EOG recordings, computed from
462 the 4 EOG channels (differences between the channels located above and below the right eye,
463 and between the channels located on the lateral side of each eye). The visually identified
464 independent components associated with eye or muscular artifacts (pre-selected with
465 *pop_icflag* function) were subsequently removed. Lastly, a final interpolation of the removed
466 channels was conducted, along with an average reference including only the EEG channels.
467 In total, 6.8% of the electrodes were interpolated, while 3.2% of the epochs and 9.1%
468 of the independent components were removed during the preprocessing procedure.
469
470 *EEG analysis*
471 We aimed to investigate whether brain activity reflects unconscious or conscious processing by
472 decoding differences in EEG dynamics in two configurations of the SQM: 1) when only a single
473 vernier is presented at different locations within the stream (V conditions), with all these
474 conditions resulting in the same percept (i.e., one perceived vernier); and 2) when two opposing
475 verniers are presented (V-AV conditions), yet there is no conscious access to the individual
476 offsets as they integrate.
477
478 *EEG decoding*
479 Linear discriminant analysis (LDA) with temporal or cross-condition generalization was used
480 to investigate neural representations related to different SQM conditions or percepts. We
481 implemented LDA with custom-made functions written in MATLAB, based on the
482 recommended settings for EEG data (Subasi & Ismail Gursoy, 2010; Grootswagers et al., 2017).
483 For each participant, LDA with temporal generalization was conducted with a leave-one-
484 pseudo-trial-out cross-validation routine (500 iterations). In each iteration, 80% of the trials
485 were sampled and combined into pseudo-trials (average of 20 trials) for the two classes, i.e.,
486 the SQM conditions, that were decoded. The mean of the training set was removed to both
487 testing and training sets, and classifier weights were estimated using a regularized covariance
488 (Ledoit & Wolf, 2004; Haufe et al., 2014; Kayser et al., 2016). The classifier weights, obtained
489 from the training set for each time point, were applied to predict the classes in the EEG data of
490 the testing set. Performance was evaluated using the area under the curve (AUC). This process
491 was repeated for each time point (cross-temporal decoding, i.e., each classifier is tested on all
492 time points), ranging from −200 to 1000 ms, with a sliding window of 7 samples corresponding
493 to a resolution of 70 ms (Grootswagers et al., 2017). LDA with cross-condition generalization

was performed similarly and with identical parameters, except that the classes used in the training sets differed from those used in the testing sets. For all decoding analyses, EEG data were resampled at 100Hz and z-scored.

We started by examining V conditions, where the presentation of a single vernier in the stream results in a clear perception of an offset. We used LDA with temporal generalization to discriminate between trials from the control condition (NV) and trials from conditions presenting one single vernier (V0, V2, or V4), irrespective of the behavioral responses (i.e., correct or incorrect report of the vernier offset). The classifiers successfully decoded the presence of information regarding the vernier, indicative of either unconscious or conscious processing (Figures 2A and 2B). We also showed some cross-condition generalization between V conditions. Using classifiers trained with V2 or V4 vs. NV conditions, we decoded V0 vs. NV conditions (Figure 2C).

Second, we explored the neural representations in the V-AV conditions, where the two opposite verniers integrate with each other. LDA with temporal generalization was used to classify between trials from the NV condition and all trials presenting two opposite verniers (V0-AV2 and V0-AV4 together), irrespective of the behavioral responses (i.e., correct or incorrect report of the 1st vernier offset). If V-AV and NV conditions cannot be discriminated, it might suggest that significant decoding reflects only neural correlates of a clearly visible vernier offset: as the two opposite verniers cancel each other out, only a straight line would be perceived, akin to the NV condition. This does not appear to be the case as the decoder successfully discriminated between these conditions (Figure 4A; see also Supplementary Figure 1 for a demonstration of cross-condition generalization between V and V-AV conditions). However, we were able to decode between V0 and V0-AV2 or V0-AV4 conditions, as well as between the two V-AV conditions, indicating that unconscious processing also contributes to this significant decoding (Figure 4A).

Lastly, we conducted an LDA analysis with temporal generalization to decode between correct and incorrect reports of the offset within each condition presenting one vernier (V0, V2, and V4; Figure 5A). This analysis aimed to specifically identify neural correlates that reflect conscious perception. All parameters remained consistent with those listed above, except for the averaging of trials for pseudo-trials, which was adjusted to 4 due to the reduced number of available trials, especially the incorrect trials (comprising only ~30% of the total for each condition).

Statistical evaluation of decoding analyses

For all decoding analyses, either with temporal or cross-condition generalization, the statistical evaluation of the 2D matrices of cross-temporal decoding results (subjects x time x time) employed cluster-based permutation approaches and surrogate analysis, following established methodologies (Nichols & Holmes, 2002; Maris & Oostenveld, 2007; Kayser et al., 2016). Clusters were defined as consecutive time points where the decoding successfully exceeded chance levels (chance = 0.5, paired t-test with $\alpha = 0.05$). The cumulative t-values within each cluster were then compared to the maximum sum derived from surrogate clusters (permutations = 10'000). Time points were considered statistically significant if the probability in the surrogate data was <0.05 for the corresponding clusters.

EEG activation patterns

We estimated activation patterns from the LDA classifiers by projecting the EEG data onto the decoder weights and normalizing the result by the dot product of the weights (Haufe et al., 2014; Grootswagers et al., 2017; Park & Kayser, 2019). We assessed the temporal dynamics of the activation patterns in the context of each decoding analysis (V0, V2, or V4 vs. NV, Figure 3A; V0-AV2/V0-AV4 vs. NV, V0-AV2/V0-AV4 vs. V0, V0-AV2 vs. V0-AV4, Figure 4A; correct vs. incorrect reports in V0, V2, and V4, Figure 5A). For each subject, we extracted the activation patterns over the significant time points. We then computed dissimilarity matrices between these activation patterns using the following procedure. First, we averaged the activation maps across subjects and standardized the average maps (z-scored). Next, we computed a map dissimilarity index at each time point by estimating the dissimilarity between the map at that time point and the maps at all other time points within the significant window. Dissimilarity was quantified using Euclidean distance, defined as the square root of the sum of squared differences between the corresponding z-scored activation maps. This process was repeated across all time points to generate a time-by-time dissimilarity matrix. To identify stable patterns—highly similar and persistent maps across time points—we employed a generalization of the Louvain community detection algorithm (Blondel et al., 2008; Rubinov & Sporns, 2010). This approach was applied to an adjacency matrix derived from the dissimilarity results, with edges defined as pairs of time points where the dissimilarity between two maps was less than the median value of the entire matrix. In this context, the Louvain community detection algorithm was used to detect clusters of time points within a graph representation of the

dissimilarity matrices, where EEG maps exhibited similar activation patterns (Figures 3A and 4B).

Topographies of the main activation patterns were then generated by averaging over temporal windows corresponding to the identified clusters (Figures 3B and 4C), or over the entire significant decoding window if no cluster was found (Figures 4C and 5B). Finally, when two different topographies were found, we correlated the spatial patterns of the topographies and the temporal dynamics of EEG activation patterns (back-projected time courses) to assess their temporal relationship and their contributions to the overall temporal dynamics (Figures 3C and 4D).

References

Ablin, P., Cardoso, J.-F., & Gramfort, A. (2017a). *Faster ICA under orthogonal constraint*. https://doi.org/10.48550/ARXIV.1711.10873

Ablin, P., Cardoso, J.-F., & Gramfort, A. (2017b). *Faster independent component analysis by preconditioning with Hessian approximations*. https://doi.org/10.48550/ARXIV.1706.08171

Aru, J., Bachmann, T., Singer, W., & Melloni, L. (2012). Distilling the neural correlates of consciousness. *Neuroscience & Biobehavioral Reviews*, *36*(2), 737–746. https://doi.org/10.1016/j.neubiorev.2011.12.003

Baars, B. J. (2002). The conscious access hypothesis: Origins and recent evidence. *Trends in Cognitive Sciences*, *6*(1), 47–52. https://doi.org/10.1016/S1364-6613(00)01819-2

Bach, M. (1996). The Freiburg Visual Acuity Test—Automatic Measurement of Visual Acuity: *Optometry and Vision Science*, *73*(1), 49–53. https://doi.org/10.1097/00006324-199601000-00008

Blondel, V. D., Guillaume, J.-L., Lambiotte, R., & Lefebvre, E. (2008). Fast unfolding of communities in large networks. *Journal of Statistical Mechanics: Theory and Experiment*, *2008*(10), P10008. https://doi.org/10.1088/1742-5468/2008/10/P10008

Brainard, D. H. (1997). The Psychophysics Toolbox. *Spatial Vision*, *10*(4), 433–436.

Cohen, M. A., Keefe, J., & Brady, T. F. (2023). Perceptual Awareness Occurs Along a Graded Continuum: No Evidence of All-or-None Failures in Continuous Reproduction Tasks. *Psychological Science*, *34*(9), 1033–1047. https://doi.org/10.1177/09567976231186798

Dainton, B. (2023). *Temporal Consciousness*. https://plato.stanford.edu/archives/spr2023/entries/consciousness-temporal/

de Cheveigné, A., & Arzounian, D. (2018). Robust detrending, rereferencing, outlier detection, and inpainting for multichannel data. *NeuroImage*, *172*, 903–912. https://doi.org/10.1016/j.neuroimage.2018.01.035

Dehaene, S., & Changeux, J.-P. (2011). Experimental and Theoretical Approaches to Conscious Processing. *Neuron*, *70*(2), 200–227. https://doi.org/10.1016/j.neuron.2011.03.018

Dehaene, S., Changeux, J.-P., Naccache, L., Sackur, J., & Sergent, C. (2006). Conscious, preconscious, and subliminal processing: A testable taxonomy. *Trends in Cognitive Sciences*, *10*(5), 204–211. https://doi.org/10.1016/j.tics.2006.03.007

Delorme, A., & Makeig, S. (2004). EEGLAB: An open source toolbox for analysis of single-trial EEG dynamics including independent component analysis. *Journal of Neuroscience Methods*, *134*(1), 9–21. https://doi.org/10.1016/j.jneumeth.2003.10.009

Delorme, A., Mullen, T., Kothe, C., Akalin Acar, Z., Bigdely-Shamlo, N., Vankov, A., & Makeig, S. (2011). EEGLAB, SIFT, NFT, BCILAB, and ERICA: New Tools for Advanced EEG Processing. *Computational Intelligence and Neuroscience*, *2011*, 1–12. https://doi.org/10.1155/2011/130714

Doerig, A., Scharnowski, F., & Herzog, M. H. (2019). Building perception block by block: A response to Fekete *et al. Neuroscience of Consciousness*, *2019*(1). https://doi.org/10.1093/nc/niy012

Drissi-Daoudi, L., Doerig, A., & Herzog, M. H. (2019). Feature integration within discrete time windows. *Nature Communications*, *10*(1), 4901. https://doi.org/10.1038/s41467-019-12919-7

Fahrenfort, J. J., Van Leeuwen, J., Olivers, C. N. L., & Hogendoorn, H. (2017). Perceptual integration without conscious access. *Proceedings of the National Academy of Sciences*, *114*(14), 3744–3749. https://doi.org/10.1073/pnas.1617268114

Fiebelkorn, I. C., Foxe, J. J., Schwartz, T. H., & Molholm, S. (2010). Staying within the lines:

The formation of visuospatial boundaries influences multisensory feature integration. *European Journal of Neuroscience*, *31*(10), 1737–1743. https://doi.org/10.1111/j.1460-9568.2010.07196.x

Grootswagers, T., Wardle, S. G., & Carlson, T. A. (2017). Decoding Dynamic Brain Patterns from Evoked Responses: A Tutorial on Multivariate Pattern Analysis Applied to Time Series Neuroimaging Data. *Journal of Cognitive Neuroscience*, *29*(4), 677–697. https://doi.org/10.1162/jocn_a_01068

Harris, J. A., McMahon, A. R., & Woldorff, M. G. (2013). Disruption of Visual Awareness during the Attentional Blink Is Reflected by Selective Disruption of Late-stage Neural Processing. *Journal of Cognitive Neuroscience*, *25*(11), 1863–1874. https://doi.org/10.1162/jocn_a_00443

Haufe, S., Meinecke, F., Görgen, K., Dähne, S., Haynes, J.-D., Blankertz, B., & Bießmann, F. (2014). On the interpretation of weight vectors of linear models in multivariate neuroimaging. *NeuroImage*, *87*, 96–110. https://doi.org/10.1016/j.neuroimage.2013.10.067

Herzog, M. H., Drissi-Daoudi, L., & Doerig, A. (2020). All in Good Time: Long-Lasting Postdictive Effects Reveal Discrete Perception. *Trends in Cognitive Sciences*, *24*(10), 826–837. https://doi.org/10.1016/j.tics.2020.07.001

Herzog, M. H., Kammer, T., & Scharnowski, F. (2016). Time Slices: What Is the Duration of a Percept? *PLOS Biology*, *14*(4), e1002433. https://doi.org/10.1371/journal.pbio.1002433

Kayser, S. J., McNair, S. W., & Kayser, C. (2016). Prestimulus influences on auditory perception from sensory representations and decision processes. *Proceedings of the National Academy of Sciences*, *113*(17), 4842–4847. https://doi.org/10.1073/pnas.1524087113

Koivisto, M., & Revonsuo, A. (2010). Event-related brain potential correlates of visual awareness. *Neuroscience & Biobehavioral Reviews*, *34*(6), 922–934. https://doi.org/10.1016/j.neubiorev.2009.12.002

Kolers, P. A., & Von Grünau, M. (1976). Shape and color in apparent motion. *Vision Research*, *16*(4), 329–335. https://doi.org/10.1016/0042-6989(76)90192-9

Lamme, V. A. F. (2006). Towards a true neural stance on consciousness. *Trends in Cognitive Sciences*, *10*(11), 494–501. https://doi.org/10.1016/j.tics.2006.09.001

Lamme, V. A. F., & Roelfsema, P. R. (2000). The distinct modes of vision offered by feedforward and recurrent processing. *Trends in Neurosciences*, *23*(11), 571–579. https://doi.org/10.1016/S0166-2236(00)01657-X

Ledoit, O., & Wolf, M. (2004). A well-conditioned estimator for large-dimensional covariance matrices. *Journal of Multivariate Analysis*, *88*(2), 365–411. https://doi.org/10.1016/S0047-259X(03)00096-4

Maris, E., & Oostenveld, R. (2007). Nonparametric statistical testing of EEG- and MEG-data. *Journal of Neuroscience Methods*, *164*(1), 177–190. https://doi.org/10.1016/j.jneumeth.2007.03.024

Marti, S., & Dehaene, S. (2017). Discrete and continuous mechanisms of temporal selection in rapid visual streams. *Nature Communications*, *8*(1), 1955. https://doi.org/10.1038/s41467-017-02079-x

McWalter, R., & McDermott, J. H. (2019). Illusory sound texture reveals multi-second statistical completion in auditory scene analysis. *Nature Communications*, *10*(1), 5096. https://doi.org/10.1038/s41467-019-12893-0

Menétrey, M. Q., Herzog, M. H., & Pascucci, D. (2023). Pre-stimulus alpha activity modulates long-lasting unconscious feature integration. *NeuroImage*, *278*, 120298. https://doi.org/10.1016/j.neuroimage.2023.120298

Mudrik, L., Breska, A., Lamy, D., & Deouell, L. Y. (2011). Integration Without Awareness: Expanding the Limits of Unconscious Processing. *Psychological Science*, *22*(6), 764–770.

https://doi.org/10.1177/0956797611408736

Nichols, T. E., & Holmes, A. P. (2002). Nonparametric permutation tests for functional neuroimaging: A primer with examples. *Human Brain Mapping*, *15*(1), 1–25. https://doi.org/10.1002/hbm.1058

Noorman, S., Stein, T., Fahrenfort, J. J., & Van Gaal, S. (2024). *Distinct neural mechanisms underlying perceptual and attentional impairments of conscious access*. https://doi.org/10.7554/eLife.97900.1

Otto, T. U. (2006). The flight path of the phoenixVThe visible trace of invisible elements in human vision. *Journal of Vision*, 8.

Otto, T. U., Ögmen, H., & Herzog, M. H. (2009). Feature integration across space, time, and orientation. *Journal of Experimental Psychology: Human Perception and Performance*, *35*(6), 1670–1686. https://doi.org/10.1037/a0015798

Otto, T. U., Ogmen, H., & Herzog, M. H. (2010). Attention and non-retinotopic feature integration. *Journal of Vision*, *10*(12), 8–8. https://doi.org/10.1167/10.12.8

Pang, D. K. F., & Elntib, S. (2021). Strongly masked content retained in memory made accessible through repetition. *Scientific Reports*, *11*(1), 10284. https://doi.org/10.1038/s41598-021-89512-w

Pang, D. K. F., & Elntib, S. (2023). Further evidence and theoretical framework for a subliminal sensory buffer store (SSBS). *Consciousness and Cognition*, *107*, 103452. https://doi.org/10.1016/j.concog.2022.103452

Park, H., & Kayser, C. (2019). Shared neural underpinnings of multisensory integration and trial-by-trial perceptual recalibration in humans. *eLife*, *8*, e47001. https://doi.org/10.7554/eLife.47001

Polich, J. (2007). Updating P300: An integrative theory of P3a and P3b. *Clinical Neurophysiology*, *118*(10), 2128–2148. https://doi.org/10.1016/j.clinph.2007.04.019

Rimsky-Robert, D., Störmer, V., Sackur, J., & Sergent, C. (2019). Retrospective auditory cues can improve detection of near-threshold visual targets. *Scientific Reports*, *9*(1), 18966. https://doi.org/10.1038/s41598-019-55261-0

Rubinov, M., & Sporns, O. (2010). Complex network measures of brain connectivity: Uses and interpretations. *NeuroImage*, *52*(3), 1059–1069. https://doi.org/10.1016/j.neuroimage.2009.10.003

Rutiku, R., Martin, M., Bachmann, T., & Aru, J. (2015). Does the P300 reflect conscious perception or its consequences? *Neuroscience*, *298*, 180–189. https://doi.org/10.1016/j.neuroscience.2015.04.029

Scharnowski, F., Ruter, J., Jolij, J., Hermens, F., Kammer, T., & Herzog, M. H. (2009). Long-lasting modulation of feature integrationby transcranial magnetic stimulation. *Journal of Vision*, *9*(6), 1–1. https://doi.org/10.1167/9.6.1

Sergent, C. (2018). The offline stream of conscious representations. *Philosophical Transactions of the Royal Society B: Biological Sciences*, *373*(1755), 20170349. https://doi.org/10.1098/rstb.2017.0349

Sergent, C., Baillet, S., & Dehaene, S. (2005). Timing of the brain events underlying access to consciousness during the attentional blink. *Nature Neuroscience*, *8*(10), 1391–1400. https://doi.org/10.1038/nn1549

Silverstein, B. H., Snodgrass, M., Shevrin, H., & Kushwaha, R. (2015). P3b, consciousness, and complex unconscious processing. *Cortex*, *73*, 216–227. https://doi.org/10.1016/j.cortex.2015.09.004

Stiles, N. R. B., Li, M., Levitan, C. A., Kamitani, Y., & Shimojo, S. (2018). What you saw is what you will hear: Two new illusions with audiovisual postdictive effects. *PLOS ONE*, *13*(10), e0204217. https://doi.org/10.1371/journal.pone.0204217

Storm, J. F., Boly, M., Casali, A. G., Massimini, M., Olcese, U., Pennartz, C. M. A., & Wilke, M. (2017). Consciousness Regained: Disentangling Mechanisms, Brain Systems, and Behavioral Responses. *The Journal of Neuroscience*, *37*(45), 10882–10893. https://doi.org/10.1523/JNEUROSCI.1838-17.2017

Subasi, A., & Ismail Gursoy, M. (2010). EEG signal classification using PCA, ICA, LDA and support vector machines. *Expert Systems with Applications*, *37*(12), 8659–8666. https://doi.org/10.1016/j.eswa.2010.06.065

Taylor, M. M., & Creelman, C. D. (1967). PEST: Efficient Estimates on Probability Functions. *The Journal of the Acoustical Society of America*, *41*(4A), 782–787. https://doi.org/10.1121/1.1910407

Vogelsang, L., Drissi-Daoudi, L., & Herzog, M. H. (2023). Processing load, and not stimulus evidence, determines the duration of unconscious visual feature integration. *Communications Psychology*, *1*(1), 8. https://doi.org/10.1038/s44271-023-00011-2

Weaver, M. D., Fahrenfort, J. J., Belopolsky, A., & Van Gaal, S. (2019). Independent Neural Activity Patterns for Sensory- and Confidence-Based Information Maintenance during Category-Selective Visual Processing. *Eneuro*, *6*(1), ENEURO.0268-18.2018. https://doi.org/10.1523/ENEURO.0268-18.2018

Acknowledgements

This work was supported by the Swiss National Science Foundation (grant number 325130_204898; grant numbers PZ00P1_179988 and PZ00P1_179988/2; and grant number TMSGI1_218247).

Data and Code Availability

The data supporting the findings of this study are available on the Open Science Framework (https://osf.io/d83vs/)

Conflict of interest

The authors declare no competing financial interests.

Authors contribution statements

M.Q.M, M.H.H. and D.P. conceived the study; M.Q.M collected the data; M.Q.M and D.P. analyzed the data; M.Q.M, M.H.H. and D.P. interpreted the results; M.Q.M, M.H.H., and D.P. wrote the manuscript.

Supplementary Material

Cross-condition generalization (V-AV conditions)

To evaluate the consistency of decoding results, we conducted another set of cross-condition decoding analyses using V-AV conditions. In these analyses, we decoded V-AV conditions from NV conditions using classifiers trained on the V0 condition (vs. NV). Only V0 trials where the reported vernier offset was correct were included to ensure that any decoding results could be linked to conscious processing. Additionally, the classifiers were applied separately to both the V0-AV2 and V0-AV4 conditions, depending on whether the first vernier offset (i.e., V0) or the second vernier offset (i.e., V2 or V4) was reported. These analyses were conducted to first confirm that one vernier is always perceived in V-AV conditions, even when the reported offset does not correspond to the central vernier, and second, to assess whether the temporal delays in decoding onset—observed in V conditions (see Figures 2B and 2C)—also exist in V-AV conditions and whether they depend on the location of the reported vernier.

The cross-condition decoding results demonstrated that classifiers successfully decoded V-AV conditions from the NV condition (AUC above 0.5, cluster-based permutation test, $p < .05$; Supplementary Figure 1). This finding confirms that processing in the V-AV and NV conditions differs (see also Figure 4A) and that one single vernier is consciously perceived when two opposite verniers are presented. More interestingly, the results suggest no decoding delays, at least in the V0-AV2 condition, as a function of the reported vernier's location. Indeed, regardless of whether the offset of the first or second vernier was reported, the decoding results showed a similar time window (from ~240 ms to ~850 ms), and the significant clusters were aligned along the diagonal, demonstrating no temporal shift between the training and testing sets. This indicates that neural processes have similar temporal dynamics in the V-AV condition as in the V0 condition (see Figures 2A and 2B for comparison).

Cross-condition generalization in V-AV conditions

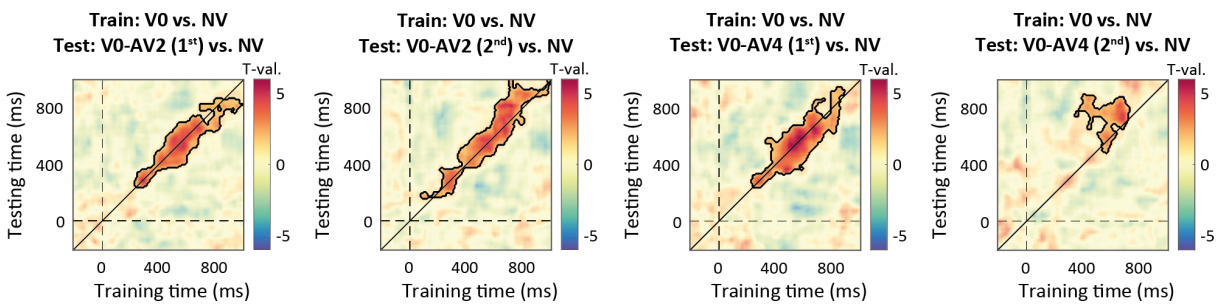

Supplementary Figure 1. Linear discriminant analysis (LDA) with cross-condition generalization in V conditions and V-AV conditions. A) Cross-condition generalization matrices demonstrate that classifiers trained with V2 or V4 vs. NV successfully discriminate between the two other conditions (V0 vs. NV and, respectively, V4 or V2 vs. NV) but with a delay. Significant clusters are highlighted (AUC above 0.5, cluster-based permutation test, $p < .05$). B) Cross-condition generalization matrices demonstrate that classifiers trained with V0 vs. NV successfully discriminate between the two V-AV conditions (V0-AV2 or V0-AV4 vs. NV), regardless of the reported vernier (1st or 2nd). Significant clusters are highlighted (AUC above 0.5, cluster-based permutation test, $p < .05$).

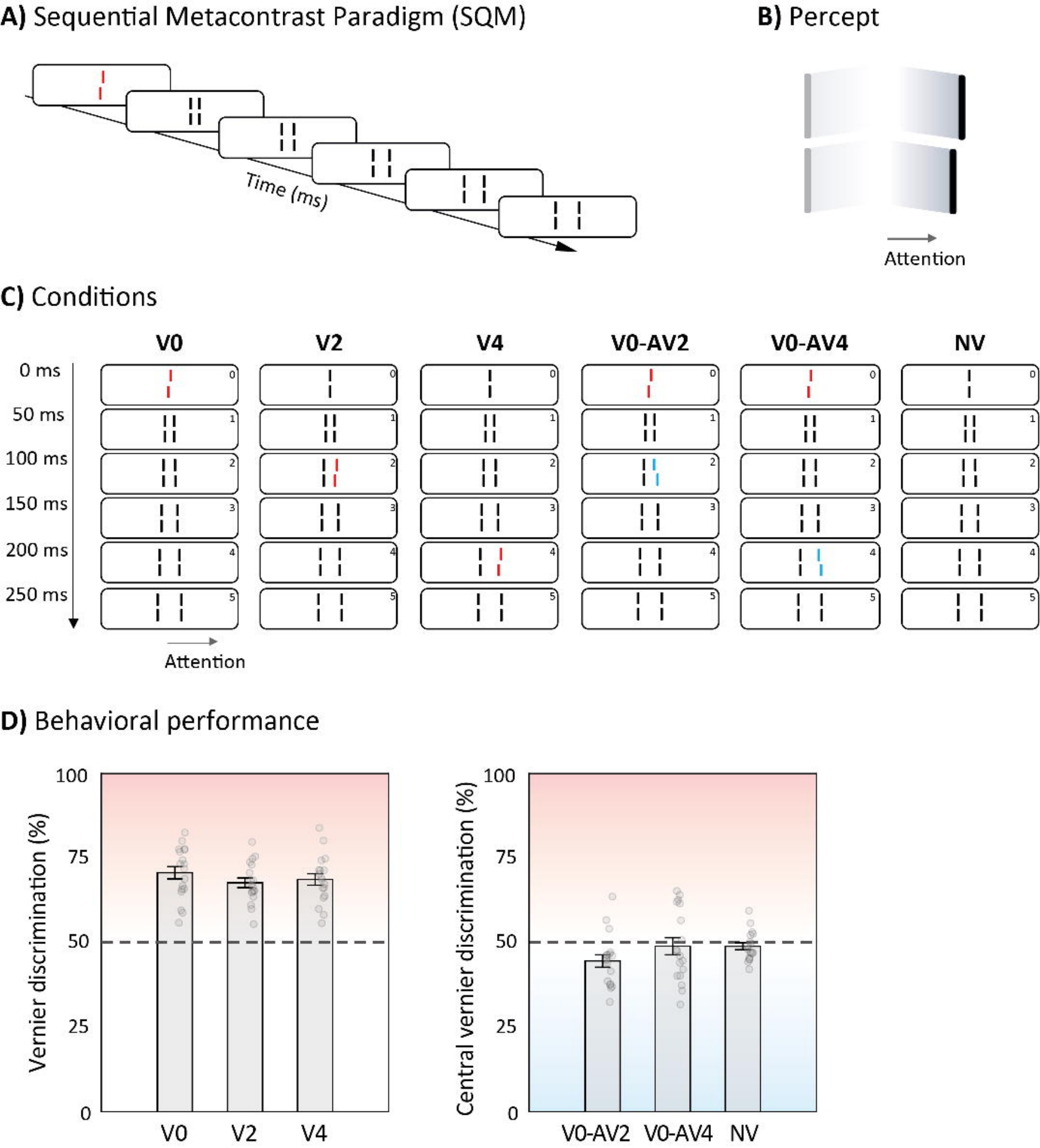
A) Sequential Metacontrast Paradigm (SQM)
Time (ms)
B) Percept
Attention
C) Conditions
V0
V2
V4
V0-AV2
V0-AV4
NV
0 ms
50 ms
100 ms
150 ms
200 ms
250 ms
Attention
D) Behavioral performance
Vernier discrimination (%)
100
75
50
25
0
V0
V2
V4
Central vernier discrimination (%)
100
75
50
25
0
V0-AV2
V0-AV4
NV

A) Temporal generalization

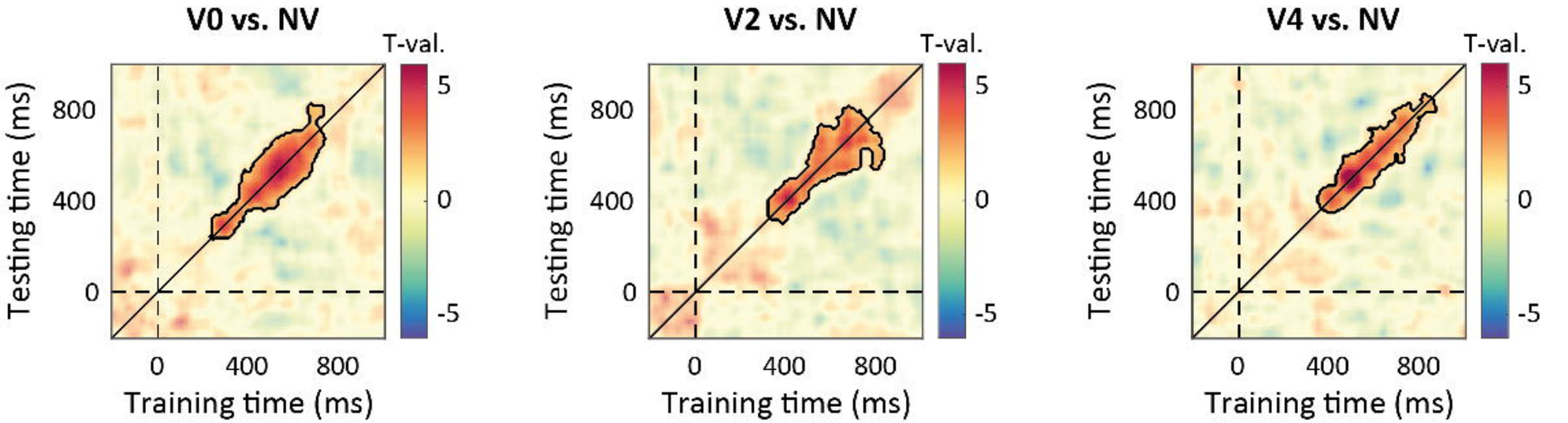

B) Diagonal decoding

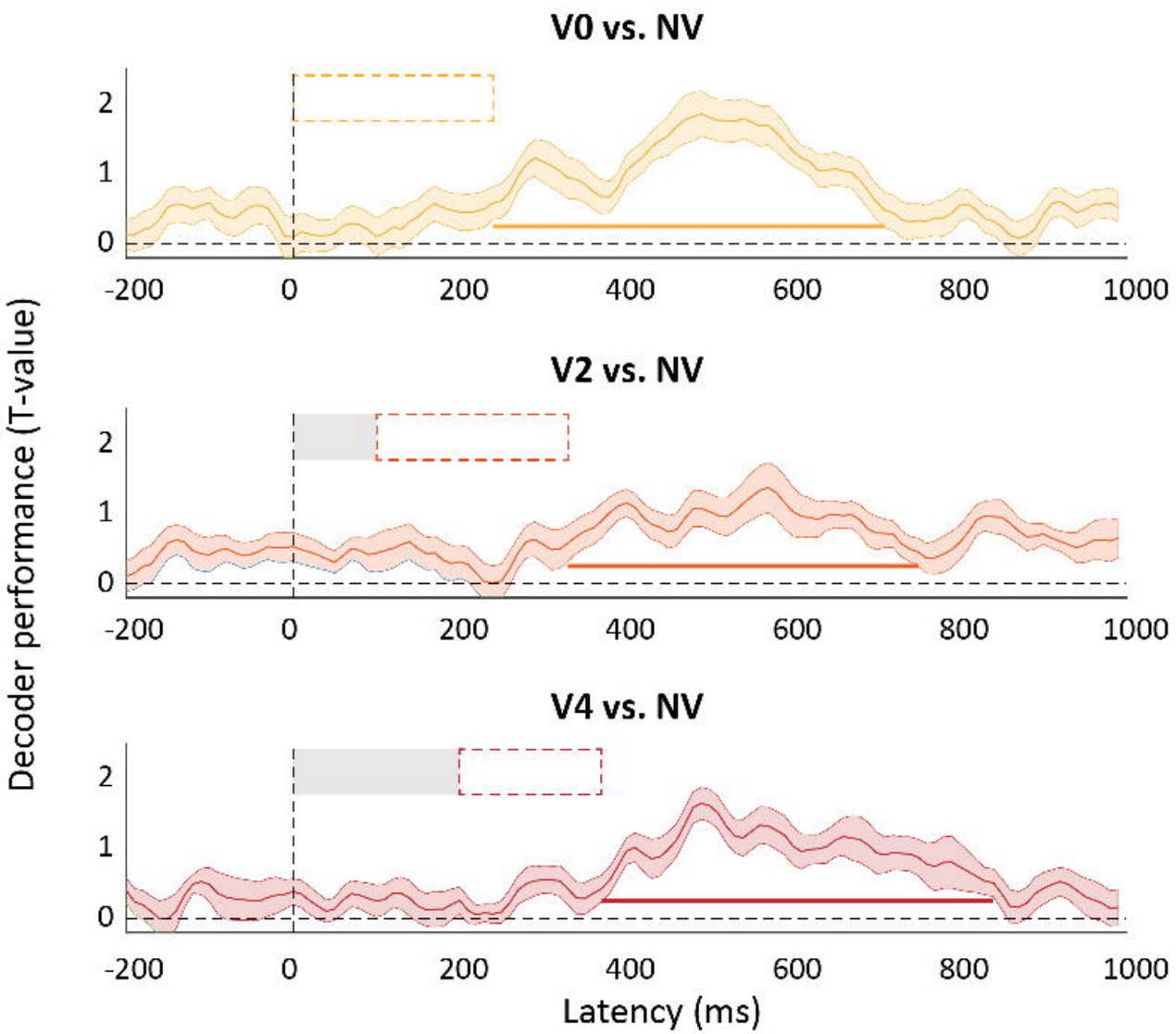

C) Cross-condition generalization

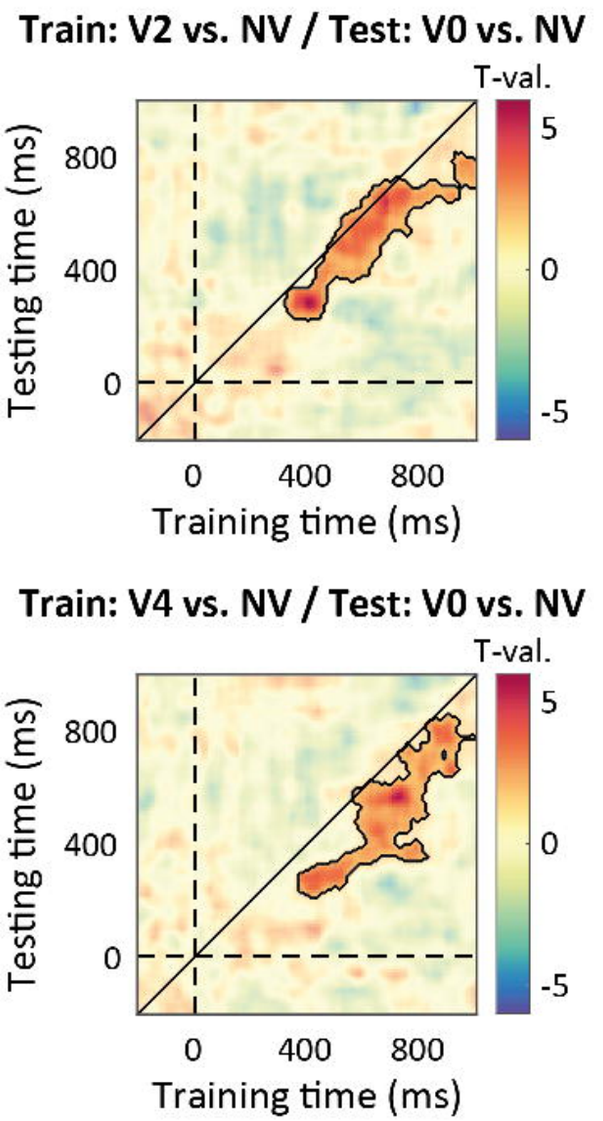

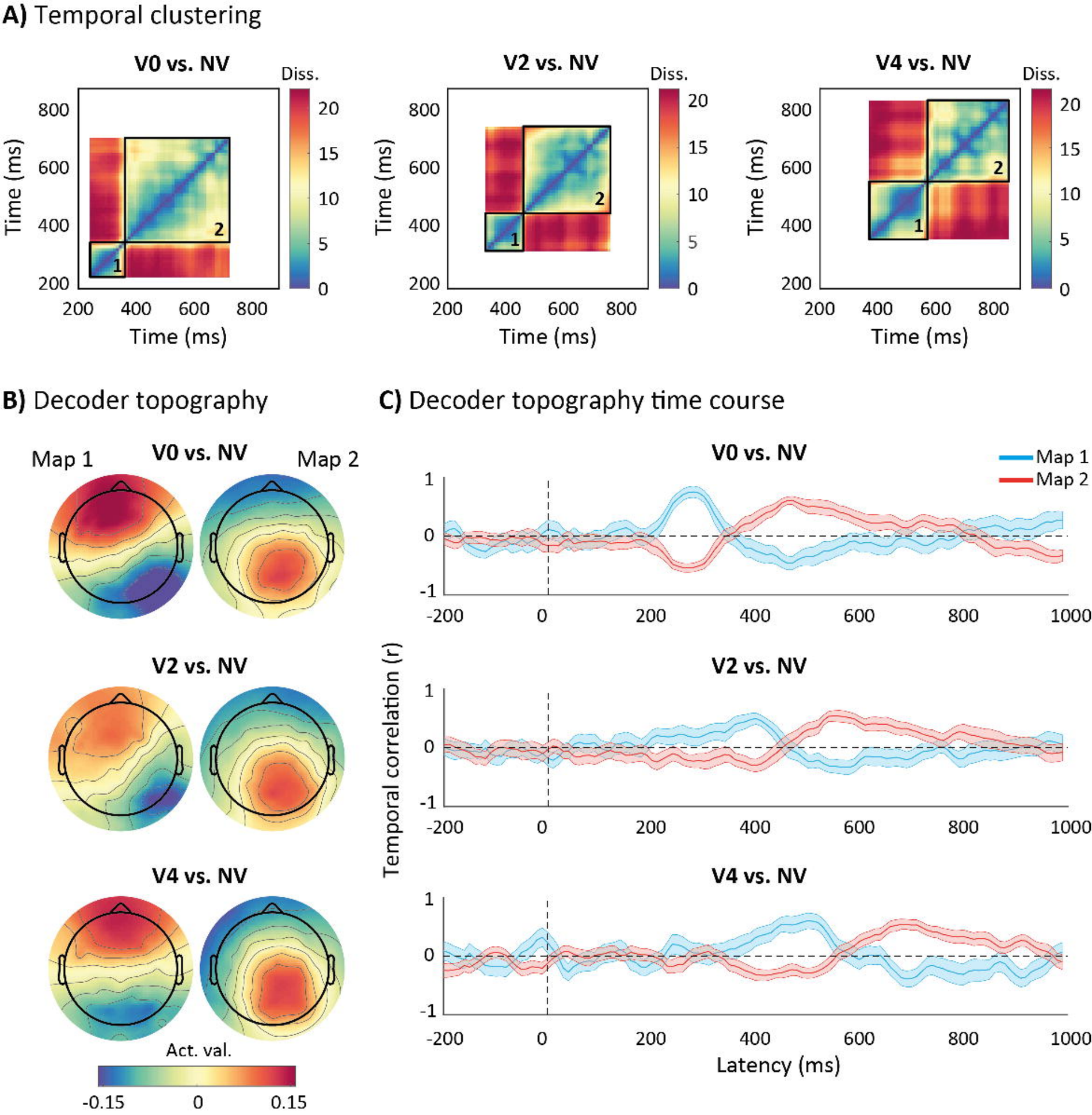
A) Temporal clustering
V0 vs. NV
V2 vs. NV
V4 vs. NV
Diss.
Time (ms)
B) Decoder topography
Map 1
Map 2
Act. val.
-0.15
0
0.15
C) Decoder topography time course
Temporal correlation (r)
Latency (ms)

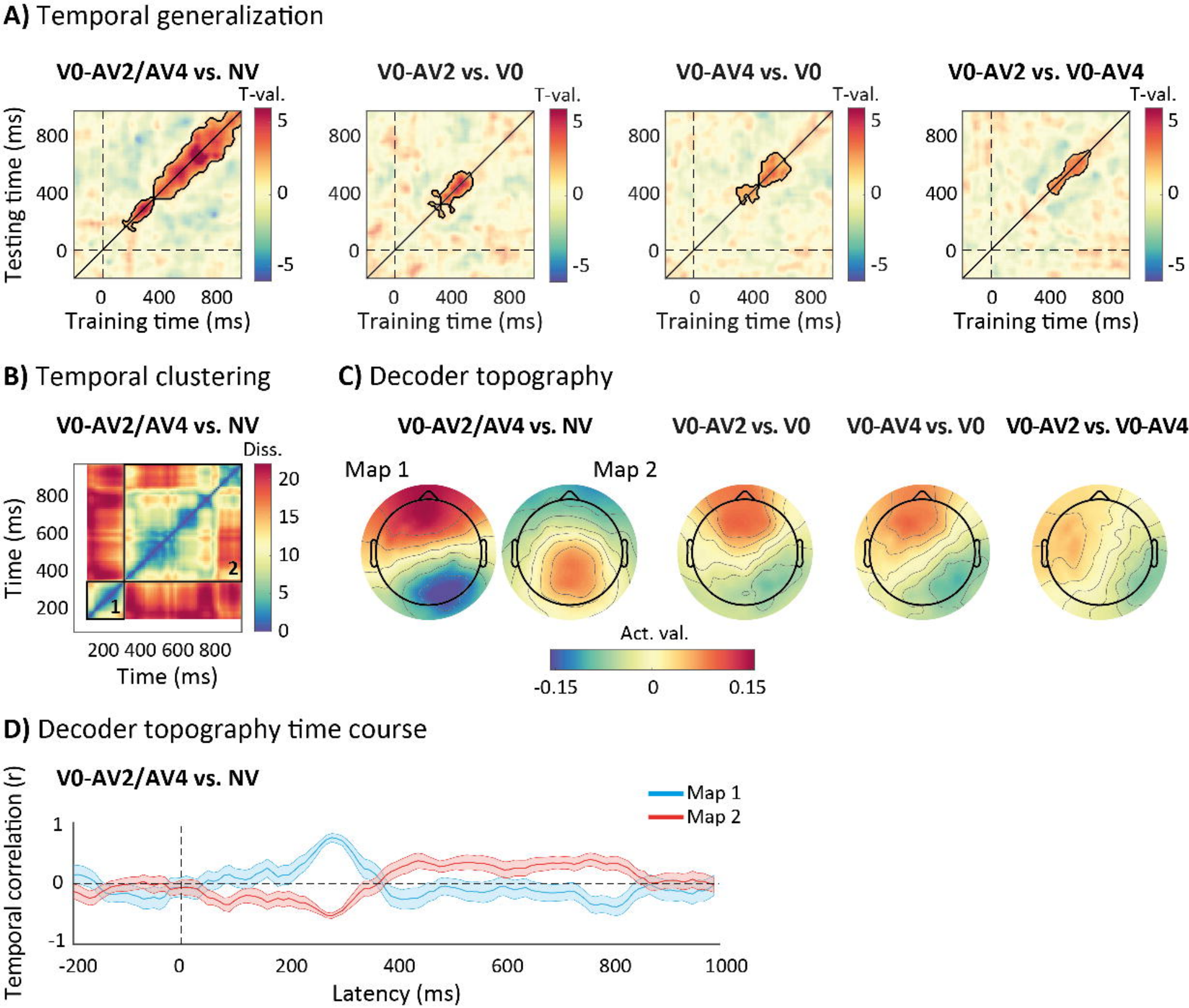
A) Temporal generalization
V0-AV2/AV4 vs. NV
V0-AV2 vs. V0
V0-AV4 vs. V0
V0-AV2 vs. V0-AV4
T-val.
5
0
-5
Testing time (ms)
800
400
0
Training time (ms)
B) Temporal clustering
V0-AV2/AV4 vs. NV
Diss.
20
15
10
5
0
Time (ms)
800
600
400
200
1
2
200 400 600 800
C) Decoder topography
V0-AV2/AV4 vs. NV
V0-AV2 vs. V0
V0-AV4 vs. V0
V0-AV2 vs. V0-AV4
Map 1
Map 2
Act. val.
-0.15
0
0.15
D) Decoder topography time course
V0-AV2/AV4 vs. NV
Map 1
Map 2
Temporal correlation (r)
1
0
-1
-200
0
200
400
600
800
1000
Latency (ms)

A) Temporal generalization

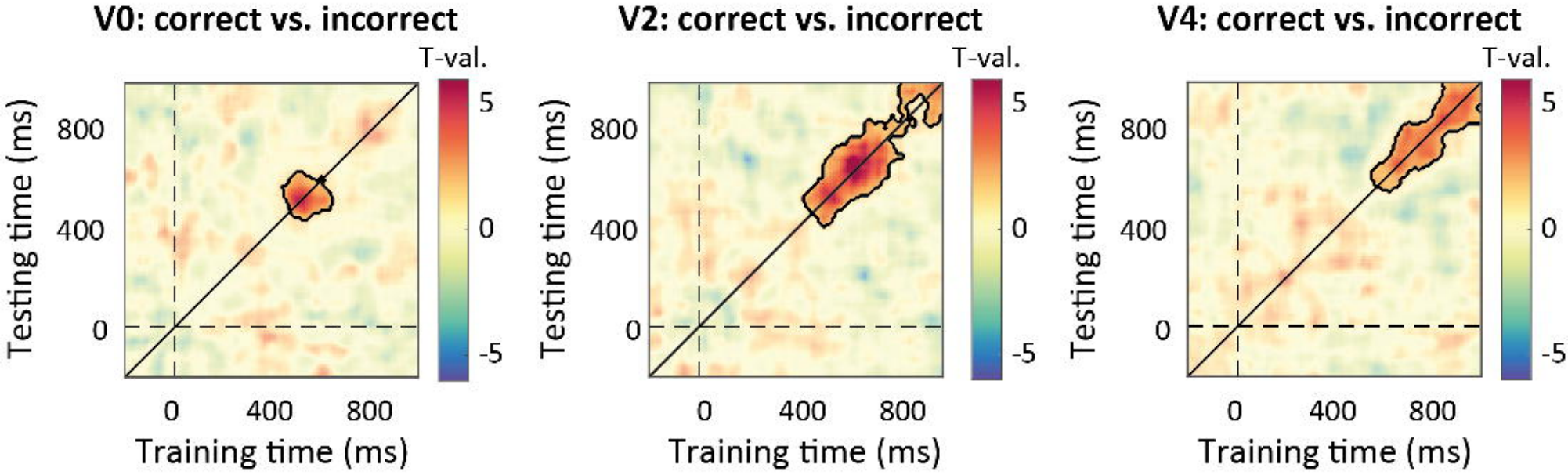
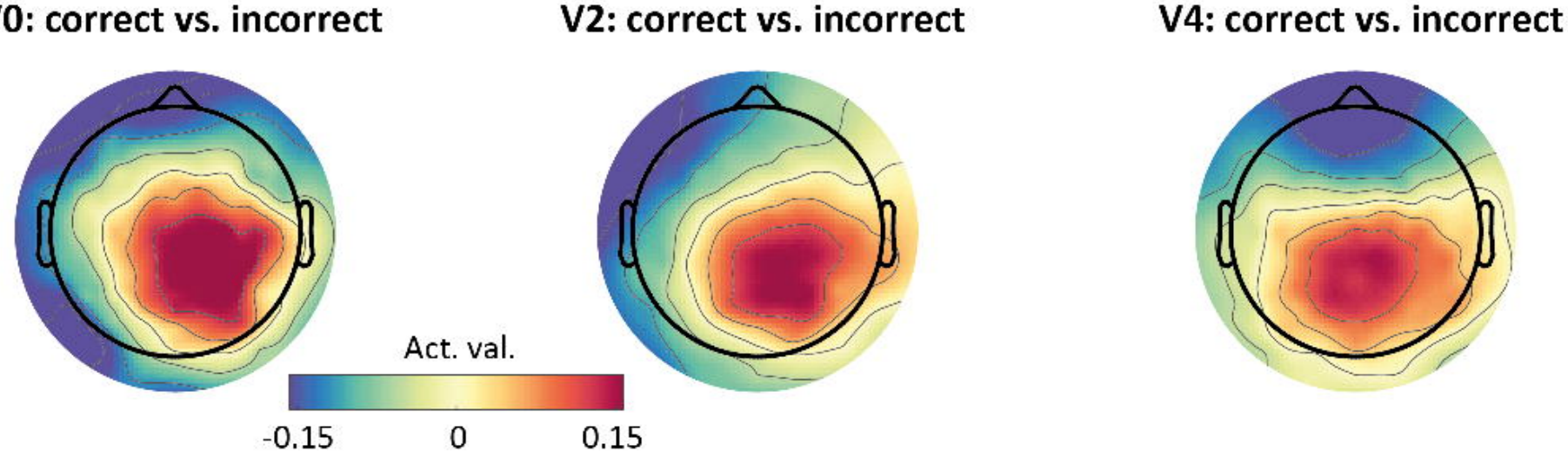
B) Decoder topography